Published in final edited form as:
Biomaterials. 2014 September ; 35(28): 8175–8185. doi:10.1016/j.biomaterials.2014.05.073.

Near-infrared fluorescence imaging of cancer mediated by tumor hypoxia and HIF1α/OATPs signaling axis

Jason Boyang Wu[a,§], **Chen Shao**[a,b,§], **Xiangyan Li**[a], **Changhong Shi**[a,c], **Qinlong Li**[a], **Peizhen Hu**[a], **Yi-Ting Chen**[a], **Xiaoliang Dou**[b], **Divya Sahu**[d], **Wei Li**[d], **Hiroshi Harada**[e], **Yi Zhang**[f], **Ruoxiang Wang**[a], **Haiyen E. Zhau**[a], and **Leland W.K. Chung**[a,*]

[a]Uro-Oncology Research Program, Department of Medicine, Cedars-Sinai Medical Center, Los Angeles, CA 90048, USA

[b]Department of Urology, Xijing Hospital, Fourth Military Medical University, Xi'an, Shaanxi 710032, China

[c]Laboratory Animal Center, Fourth Military Medical University, Xi'an, Shaanxi 710032, China

[d]Department of Dermatology, Keck School of Medicine, University of Southern California, Los Angeles, CA 90089, USA

[e]Department of Radiation Oncology and Image-Applied Therapy, Kyoto University Graduate School of Medicine, Kyoto 606-8507, Japan

[f]Biomedical Imaging Research Institute, Cedars-Sinai Medical Center, Los Angeles, CA 90048, USA

Abstract

Near-infrared fluorescence (NIRF) imaging agents are promising tools for noninvasive cancer imaging. Here, we explored the mechanistic properties of a specific group of NIR heptamethine carbocyanines including MHI-148 dye we identified and synthesized, and demonstrated these dyes to achieve cancer-specific imaging and targeting via a hypoxia-mediated mechanism. We found that cancer cells and tumor xenografts exhibited hypoxia-dependent MHI-148 dye uptake *in vitro* and *in vivo*, which was directly mediated by hypoxia-inducible factor 1α (HIF1α). Microarray analysis and dye uptake assay further revealed a group of hypoxia-inducible organic anion-transporting polypeptides (OATPs) responsible for dye uptake, and the correlation between OATPs and HIF1α was manifested in progressive clinical cancer specimens. Finally, we demonstrated increased uptake of MHI-148 dye *in situ* in perfused clinical tumor samples with activated HIF1α/OATPs signaling. Our results establish these NIRF dyes as potential tumor

*Corresponding Author. Uro-Oncology Research Program, Cedars-Sinai Medical Center, 8750 Beverly Blvd., Atrium 103, Los Angeles, CA 90048, USA. Tel.: +1 310 4237622. Leland.Chung@cshs.org.
§These authors contributed equally to this work.

hypoxia-dependent cancer-targeting agents and provide a mechanistic rationale for continued development of NIRF imaging agents for improved cancer detection, prognosis and therapy.

Keywords

cancer imaging; HIF1α; hypoxia; near-infrared dyes; organic anion-transporting polypeptides

1. Introduction

Near-infrared fluorescence (NIRF) imaging has recently emerged as a useful tool for noninvasive cancer imaging [1]. NIRF agents show very limited autofluorescence from intrinsic chromophores, but upon binding to biomolecules they display drastically increased fluorescence due to rigidization of the fluorophores [2, 3]. Polymethine carbocyanine dyes, such as pentamethine and heptamethine carbocyanines, are representative NIRF contrast agents that have shown great potential for both experimental and clinical NIRF imaging [4]. These organic dyes feature high extinction coefficients and relatively large Stokes' shift, and in the presence of emission wavelengths ranging from 700–1,000 nm their fluorescence can be readily captured from deep tissues by commercially available imaging modalities [2, 3].

Most conventional approaches for utilizing NIRF dyes in cancer imaging require chemical conjugation of NIR fluorophores with appropriate tumor-specific ligands, including metabolic substrates, aptamers, growth factors, and antibodies [5–7]. A number of surface molecules have been tested as targets, including membrane receptors, extracellular matrices, cancer cell surface-specific markers, and neovascular endothelial cell-specific markers [8, 9]. These approaches have created agents with a narrower spectrum for cancer imaging since the NIRF moieties only detect specific types of cancer cells with well-characterized surface properties [10]. Moreover, the specificity and affinity of targeting ligands could also be affected by chemical conjugation [3]. Hence, there is an unmet need for developing NIRF dyes with simpler and more straightforward use to advance noninvasive cancer imaging, taking into account the heterogeneous nature of cancer.

We previously identified and synthesized a specific class of NIRF heptamethine carbocyanines as dual imaging and cancer targeting agents. Two prototypic heptamethine carbocyanine dyes including MHI-148 demonstrated promising biological activity [11, 12]. However, how these dyes achieve cancer-specific targeting properties are largely unclear. Tumor cells, though display heterogeneity in general, still share select common features for proliferation and survival such as responses to environmental hypoxic stimuli through certain epigenetic alterations. In this study, utilizing genitourinary cancers as a model system, we investigated the intrinsic features of these dyes by linking the dye uptake with tumor hypoxia and explored the possible molecular mechanisms that may mediate the preferential uptake of this class of NIRF dyes by cancer cells.

2. Materials and methods

2.1. Cell culture and reagents

The human prostate cancer (PCa) cell lines PC-3, PC-3M and LNCaP, human breast cancer cell line MDA-MB-231, and human leukemia cell line K562 were purchased from American Type Culture Collection (ATCC, Manassas, VA). The normal prostatic epithelial PrEC cells were purchased from Lonza (Allendale, NJ). The human PCa cell lines C4-2, $ARCaP_E$ and $ARCaP_M$ were established by our laboratory [13–15], and the murine prostate cancer cell line MPC3 was kindly provided by Dr. Neil Bhowmick (Cedars-Sinai Medical Center, Los Angeles, CA) [16]. For hypoxia treatment, cells were grown in a hypoxic chamber (1% O_2, 5% CO_2). PC-3 cells stably overexpressing *5HREp-ODD-luc* were established by lipofectamine-mediated transfection of the construct followed by 2-week G418 (500 μg/ml) selection as described previously [17]. PC-3 cells overexpressing a constitutively active *HIF1α* construct were established by retroviral infection as described previously [18]. *HIF1α, OATP1B3* and non-targeting control shRNA lentiviral particles used to establish stable knockdown cell lines were purchased from Santa Cruz (Santa Cruz, CA). The heptamethine carbocyanine MHI-148 dye was synthesized and purified as described previously [11]. Cobalt chloride, rifampicin, gemfibrozil and bromosulfophthalein were purchased from Sigma-Aldrich (St. Louis, MO). DMOG was purchased from Millipore (Billerica, MA).

2.2. Tumor xenograft studies

Male 4- to 6-week-old athymic nude mice were purchased from Taconic (Oxnard, CA), housed in the animal research facility at Cedars-Sinai Medical Center (CSMC), and fed a normal chow diet. For xenograft studies, 1×10^6 cells were injected subcutaneously into nude mice. Each mouse was injected on either one or both flanks, and at least five mice were used for each group. Tumors were dissected 4–6 weeks after inoculation and fixed in 4% formaldehyde and embedded in paraffin for subsequent histological analysis.

2.3. Clinical specimens

Archival formalin-fixed paraffin-embedded (FFPE) PCa clinical specimens were obtained from the Department of Pathology, Xijing Hospital, Fourth Military Medical University (FMMU). All renal cell carcinoma (RCC) patients enrolled in the present study were from the Department of Urology, Xijing Hospital, FMMU, and the exclusion criteria included kidney cysts, renal pelvis carcinoma and other inflammatory diseases.

2.4. Analysis of NIRF dye uptake in cancer cells, tumor xenografts and clinical tumor specimens

2.4.1. Cancer cell model—After exposure to different treatments, cells were incubated with MHI-148 dye at a concentration of 5 μM at 37°C for 10 min and washed twice with PBS to remove excess dyes. Cells were fixed in 10% formaldehyde and subjected to analysis of NIRF dye uptake by a BD Accuri C6 flow cytometer (BD Biosciences, San Jose, CA) equipped with a 780/30 nm filter for NIRF detection, and the data was analyzed by FlowJo software (Tree Star Inc., Ashland, OR).

2.4.2. Tumor xenograft model—Mice bearing xenografted tumors, when tumor sizes reached 2–6 mm in diameter assessed by palpation, were injected intraperitoneally with MHI-148 dye at a dose of 50 nmol/mouse. Whole-body or organ-specific optical imaging was taken at 24 hour using an IVIS Lumina XR imaging system (PerkinElmer, Waltham, MA) equipped with fluorescent filter sets (excitation/emission, 783/840 nm) as described previously [11, 12].

2.4.3. Clinical RCC specimens—RCC patients who were histopathologically confirmed underwent complete retroperitoneal laparoscopic nephrectomy. Immediately subsequent to the surgical removal, the kidney was administered intra-arterially with 5000 units of heparin for anti-coagulation, and then subjected to perfusion with 300 ml saline at a rate of 20 ml/min at 4°C. Next, the kidney was perfused with MHI-148 dye (0.5 nmol/g) in 500 ml saline at a rate of 20 ml/min at 4°C, and further infused with 500 ml Ringer's solution to remove excess dyes. Uptake of MHI-148 dye in the kidney was determined by NIRF imaging as described in 2.4.2. RCC and adjacent normal tissues were further excised and cut into small blocks followed by NIRF imaging and signal intensity quantification. All procedures were performed either on ice or at 4°C.

2.5. Luciferase assay and bioluminescence imaging

PC-3 cells that stably carry *5HREp-ODD-luc* after receiving different treatments were subjected to cell lysis, and the cell lysates were incubated with D-luciferin (Promega, Madison, WI) for luciferase readout using a Monolight luminometer (BD Biosciences) as described previously [17]. Bioluminescence imaging of either PC-3 cells or tumor xenografts that carry *5HREp-ODD-luc* after receiving D-luciferin (3 mg/mouse via intraperitoneal delivery) was performed using a Xenogen IVIS Spectrum imaging system (PerkinElmer).

2.6. Immunohistochemical (IHC) and double quantum dot labeling (QDL) analysis of tumor xenograft and clinical tumor specimens

FFPE tissue specimens were stained with antibodies specific for HIF1α (1:30) (H1alpha67, Novus Biologicals, Littleton, CO or 54, BD Bioscience), VEGF-A (1:40) (A-20, Santa Cruz), or OATP1B3 (1:50, Sigma-Aldrich or 1: 30, H-52, Santa Cruz) by IHC or double QDL as described previously [19].

2.7. cDNA microarray analysis

RNA samples were prepared from control and constitutively active HIF1α overexpressing PC-3 cells using a RNeasy Mini kit (Qiagen, Valencia, CA) and processed for cDNA microarray analysis. Human U133plus2.0 array hybridizations were performed by the University of California, Los Angeles (UCLA) Clinical Microarray Core following the standard Affymetrix GeneChip Expression Analysis protocol. The acquisition of array images was undertaken using the Affymetrix GeneChip Command Console 1.1 (AGCC).

2.8. Biochemical analyses

Total RNA was isolated using a RNeasy Mini kit and reverse-transcribed to cDNA using M-MLV reverse transcriptase (Promega) as described previously [17, 20]. qPCR was conducted using SYBR Green PCR Master Mix and run with Applied Biosystems 7500 Fast Real-Time PCR System (Applied Biosystems, Carlsbad, CA). PCR conditions included an initial denaturation step of 3 min at 95oC, followed by 40 cycles of PCR consisting of 30 s at 95oC, 30 s at 60oC, and 30 s at 72oC. The PCR data were analyzed by 2^{AACT} method [21]. Details on primers for qPCR are provided in Supplemental Table 2.

For immunoblotting, cells were extracted with RIPA buffer in the presence of a protease and phosphatase inhibitor cocktail (Thermo Scientific, Rockford, IL), and immunoblotting were performed as described previously [22, 23] using primary antibodies as follows: HIF1α (1:500) (54, BD Bioscience), OATP1B3 (1:500) (Sigma-Aldrich, or H-52, Santa Cruz), or β-Actin (1:2000) (AC-15, Sigma-Aldrich).

2.9. Chromatin immunoprecipitation (ChIP) analysis and qPCR

ChIP assay was used to determine the *in vivo* association of HIF1α protein with *OATP1B3* promoter in PC-3 cells treated with either vehicle or cobalt chloride (200 μM, 16 h, dissolved in PBS) by a SimpleChIP Enzymatic Chromatin IP Kit (Cell Signaling, Danvers, MA). Briefly, chromatin that was cross-linked with nuclear proteins, enzymatically digested with micrococcal nuclease and sonicated was immunoprecipitated with anti-HIF1α antibody. After being pelleted with agarose beads and purified, immunoprecipitated chromatin was subsequently subjected to qPCR with a pair of primers specifically targeting the *OATP1B3* promoter region that encompasses a HRE. IgG included in the kit was used as a negative control for IP. A control primer set for *OATP1B3* exon1 was used as a negative control for PCR. Primer sequences for the *OATP1B3* promoter were forward 5'-AAAACAATTAGCCGGGCGTTG-3' and reverse 5'-CTTATCCAGAAATCTGGTATGC-3', and for *OATP1B3* exon1 were forward 5'-ATGTTCTTGGCAGCCCTGTC-3' and reverse 5'-CAATTTCAAAGCTTCCATCAATTA-3'. Two percent of chromatin prior to IP was saved as input, and data were presented as the percent of input from three independent experiments

2.10. Statistical analysis

Data were presented as the mean ± SEM from at least three independent experiments and analyzed with an unpaired Student's t test. A *p* value less than 0.05 was considered as statistically significant.

2.11. Study approval

All animal studies received prior approval by the IACUC of CSMC and were conducted in compliance with its recommendations. All human studies were reviewed and approved by the IRB of CSMC and FMMU, and written informed consent was provided for human samples.

Results

3.1. MHI-148, a NIRF dye, targets tumor hypoxia in vivo

We sought to determine the association of tumor hypoxia with NIRF imaging of cancer cells and tumor xenografts given that hypoxia is a common condition found in a wide range of cancer cells or solid tumors [24]. At the cellular level, cancer cells within the tumors or as circulating tumor cells in contrast to normal cells can survive hypoxic conditions and show increased expression of hypoxia-inducible factors (HIFs), such as HIF1α [25]. To assess intratumoral hypoxia, we used a HIF1α-dependent reporter construct, *5HREp-ODD-luc* [26], in which 5 copies of the hypoxia-response element (HRE) enhance the expression of a luciferase (luc) protein fused with the oxygen-dependent degradation (ODD) domain under hypoxia (Fig. 1B, top panel), to monitor the hypoxic status and HIF1α activity in a real-time manner in cancer cells and tumor xenografts. Under normoxic conditions, the ODD domain of HIF1α is modified by 4-prolyl hydroxylases (PHDs) and von Hippel-Lindau tumor suppressor (VHL), which require oxygen and subsequently result in the rapid degradation of HIF1α protein. In contrast, HIF1α is stabilized under hypoxia that destroys PHD activity due to the lack of oxygen [27]. Therefore, the expression of *5HREp-ODD-luc*, by modulating the oxygen-sensitive ODD-luc fusion protein levels, produces a marginal leak of luminescence under normoxia but increases markedly under hypoxia, reflecting dynamic and real-time HIF1α activity correlating to the levels of hypoxia.

To validate this construct in the present system, we stably overexpressed *5HREp-ODD-luc* in human prostate cancer (PCa) PC-3 cells, which showed a time-dependent increase of luminescence signals in parallel with stabilized HIF1α protein under hypoxia (Fig. 1B, middle and bottom panels). These observations were further recapitulated under treatment with either cobalt chloride or dimethyloxalyglycine (DMOG), both acting as HIF1α stabilizers by inhibiting PHD activity (Fig. S1). Notably, there was barely detectable luminescence in cells either under normoxia or without the treatment (Fig. 1B and S1), suggesting the specificity of this construct for hypoxia or HIF1α activation. To determine the potential hypoxic effects on the tumor uptake of MHI-148 dye (chemical structure shown in Fig. 1A) *in vivo*, we established a subcutaneous tumor xenograft mouse model using *5HREp-ODD-luc*-overexpressing PC-3 cells and subjected mice to dual bioluminescence and fluorescence imaging. As shown in Fig. 1C (left panel), bioluminescence signals were concurrently accumulated centrally with NIRF signals of MHI-148 in tumor xenografts. Slim tumor slices (1–1.5 mm), dissected from tumor tissues immediately after whole-body optical imaging, were analyzed *ex vivo*, and superimposed bioluminescence and NIRF images were also observed (Fig. 1C, right panel). The co-registration of bioluminescence and NIRF signals in tumor xenografts suggested a correlation between tumor hypoxia and the uptake of NIRF dyes by tumors.

3.2. NIRF dye uptake by cancer cells and tumor xenografts is enhanced by hypoxia

To determine if hypoxia is responsible for the preferential uptake of NIRF dyes by cancer cells, we examined a wide spectrum of human and murine carcinomas including prostate carcinoma (PC-3, PC-3M, LNCaP, C4-2, $ARCaP_E$, $ARCaP_M$ and MPC3), breast carcinoma (MDA-MB-231), colorectal carcinoma (CT26) and leukemia (K562) cell lines under

hypoxic conditions. After exposure to hypoxia, these cells were incubated with MHI-148 dye followed by flow cytometric analysis to quantify the NIRF intensity. As shown in Fig. 2A, hypoxia increased the accumulation of MHI-148 dye in all cancer cell lines by 30% to more than 2 fold relative to their incubation under normoxic conditions. In contrast, the normal prostatic epithelial PrEC cells, serving as a negative control, did not show significant changes in dye uptake under hypoxia, which is consistent with our previous observations that normal cells retain little of these NIRF dyes [11]. We further showed that cobalt chloride treatment, a chemical mimicker of hypoxia, induced the uptake of MHI-148 dye in select cancer cells lines (PC-3, $ARCaP_E$ and MDA-MB-231) in a time-dependent manner (Fig. 2B).

To determine whether HIF1α protein directly mediates NIRF dye uptake by cancer cells, we stably introduced a constitutively active *HIF1α* expression construct (*CA-HIF1α*), which lacks the ODD domain and hence escapes degradation under normoxia, into cancer cells (PC-3, PC-3M and MDA-MB-231) by retroviral infection. Successful enforced expression of HIF1α, confirmed by immunoblotting, enhanced the ability of cancer cells to take up MHI-148 dye by more than 50% under normoxic conditions (Fig. 2C). Conversely, stable targeted silence of *HIF1α* gene expression via lentiviral shRNAs in select cancer cell lines (PC-3, PC-3M, C4-2, $ARCaP_E$ and MDA-MB-231) blunted the hypoxia-induced increase of dye uptake to lower levels comparable to those observed under normoxic conditions (Fig. 2D).

Next, we studied the hypoxic effects on the uptake of NIRF dyes in tumor-bearing mice. PC-3 cells that stably overexpressed either *CA-HIFα* construct or an empty vector were used to establish subcutaneous tumor xenografts in nude mice. Each mouse carried both control and HIF1α-overexpressing tumors with one on each flank for a simultaneous comparison of the extent of dye uptake between the tumors. We observed that tumor HIF1α protein expression correlated progressively with tumor growth, concurring with the observations from other groups [28]. To ensure that tumor size did not interfere with the assessment of tumor uptake of NIRF dyes, tumor NIRF intensity was normalized to tumor weight at the end of the study. HIF1α overexpression enhanced the uptake of MHI-148 dye by PC-3 tumor xenograft relative to control tumor, leading to a 60% increase of NIRF signals after normalization to tumor weight (Fig. 3A and 3B, left panel). On the other hand, stable knockdown of *HIF1α* via lentiviral shRNAs (shHIF1α) reduced the ability of PC-3 tumors to take up and retain MHI-148 dye by 56% subsequent to normalization of NIRF signals to tumor weight, compared with control tumor that expressed a scrambled shRNA (shCon) (Fig. 3A and 3B, right panel). The accumulation of MHI-148 dye was found specific to tumors but not normal organs including the liver, lung, spleen, kidney, heart, prostate and testis by both *in vivo* and *ex vivo* NIRF imaging modalities, reinforcing the tumor-specific targeting ability of NIRF dyes (Fig. 3A). Tumor HIF1α expression was confirmed by immunohistochemical (IHC) analysis by probing protein expression of HIF1α and its target genes, such as vascular endothelial growth factor A (VEGF-A) [24] (Fig. 3C). These data collectively suggest that hypoxia, through its key mediator HIF1α, mediates the uptake of NIRF dyes by cancer cells.

3.3. Regulation of OATPs by hypoxia and HIF1α in PCa

To elucidate the effectors downstream of the hypoxia/HIF1α-mediated signals and responsible for the preferential uptake of NIRF dyes by cancer cells, we conducted cDNA microarray analysis with control and HIF1α-overexpressing PC-3 cells. Preliminary results, confirmed later by qPCR, identified a family of organic anion-transporting polypeptide (*OATP*) genes induced by constitutive activation of HIF1α protein (Fig. 4A). OATPs represent a superfamily of solute carrier transporters. Currently there are 11 known human OATPs classified into 6 families and subfamilies on the basis of their amino acid sequence homologies. OATPs facilitate the transport of a large number of substrates, including organic acids, drugs and hormones, into cells in a highly substrate- and pathophysiologic-dependent manner [29]. Hypoxia induction of *OATPs* was further demonstrated in 4 human PCa cell lines (LNCaP, PC-3, DU-145 and $ARCaP_E$), which all showed an increasing trend of mRNA expression for most *OATPs* under hypoxia (Fig. S2A, left panel). *VEGF-A* and glucose transporter 1 (*Glut1*), known for HIF1α target genes [24], were used as a positive control for validating hypoxic effects. Considering the reported association of dysregulated expression of OATPs with cancer progression [29, 30], we conducted a survey of the expression of all OATPs in 10 human PCa cell lines. Most of *OATPs* demonstrated higher mRNA expression in PCa cells relative to normal prostatic epithelial PrEC cells (Fig. S2A, right panel).

Recent evidence has indicated the aberrant expression and genetic variants of select *OATPs*, such as *OATP1B3* [31], in different types of human cancer [30], which led us to speculate a potential regulatory link between OATPs and hypoxia signals in human cancer progression. To test this idea, we examined the protein expression of HIF1α and OATP1B3 as a representative in PCa clinical specimens with either low or high Gleason grades. We observed that the expression of both HIF1α and OATP1B3 proteins were well correlated with prostate tumor Gleason grades (Fig. 4B), which was further confirmed by double quantum dot labeling (QDL) analysis, enabling quantification of staining intensity of each protein at the single cellular level. As shown in Fig. 4C, the increased co-expression of HIF1α and OATP1B3 was progressively associated with higher Gleason grades (left and middle panels), and HIF1α protein expression further showed significant correlation with OATP1B3 expression in high-grade cancer patient samples (right panel). These data in aggregate establish a molecular correlation between HIF1α and OATP1B3 in clinical cancer settings.

To examine further the relationship between HIF1α and OATP1B3, we analyzed OATP1B3 protein and mRNA expression in PCa cells and tumor xenografts subsequent to the change of hypoxic or HIF1α protein expression levels. In response to hypoxic stimuli, both OATP1B3 protein and mRNA expression were induced in PC-3 and $ARCaP_E$ cells (Fig. 4D and 4E), which was recapitulated in cancer cells and tumor xenografts by enforced HIF1α protein expression (Fig. S2B, S2C and S2D, left panel). Conversely, stable knockdown of HIF1α protein expression reduced OATP1B3 protein and mRNA expression (Fig. S2B, S2C and S2D, right panel). To investigate whether HIF1α directly regulates *OATP1B3* gene, we attempted to identify a functional HRE in the *OATP1B3* promoter. Sequence analysis of a 2-kb DNA segment located upstream of the transcription initiation site of *OATP1B3* gene

revealed a region (-926/-923) that exhibits strong sequence identity to a canonical HRE [32] (Fig. 4F). By conducting chromatin immunoprecipitation assay coupled with qPCR analysis, we were able to detect the physical interaction of HIF1α protein with the *OATP1B3* promoter region that harbors a HRE in cobalt chloride-treated cells, whereas this association was absent in control cells (Fig. 4G). These results provide evidence that hypoxia mediates *OATP1B3* gene activation by facilitating the cis-trans interactions between a specific HRE in the *OATP1B3* promoter and HIF1α protein.

3.4. OATP1B3 mediated NIRF dye uptake by cancer cells and tumor xenografts

To investigate whether OATP1B3 directly mediates the uptake of NIRF dyes in cancer cells, we used PC-3 and $ARCaP_E$ cells, which were stably infected with either *OATP1B3*-targeting shRNAs (shOATP1B3) or a scrambled shRNA (shCon). Stable knockdown of OATP1B3 protein expression resulted in a 30% decrease in MHI-148 dye uptake by cancer cells under normoxia (Fig. 5A), indicating that OATP1B3 can mediate the transport of NIRF dyes into cancer cells in a hypoxia-independent manner. Moreover, pharmacological interference with OATP1B3 activity in cancer cells by pre-treatment with different inhibitors compromised the hypoxia-induced uptake of MHI-148 dye by up to 65% and 31% in PC-3 and $ARCaP_E$ cells, respectively (Fig. 5B). To determine the OATP1B3 effect on NIRF dye uptake by xenograft tumors, nude mice were inoculated subcutaneously with PC-3 or $ARCaP_E$ cells (shCon vs. shOATP1B3). We observed parallel growth of control and OATP1B3-knockdown tumors, suggesting that OATP1B3 did not affect cell proliferation even though its expression correlated with clinical cancer progression. Importantly, knockdown of OATP1B3 protein expression, confirmed by IHC analysis (Fig. 5C), significantly reduced MHI-148 dye intensity after normalization to tumor weight in both PC-3 and $ARCaP_E$ tumor xenografts, by 40% and 15% respectively (Fig. 5D and 5E). These results suggest that OATP1B3 directly mediates NIRF dye uptake and retention in tumors, which can be independent of hypoxia signaling.

3.5. Assessment of NIRF dye uptake and HIF1α/OATP signaling axis in clinical renal cell carcinoma (RCC) samples

A critical issue that arises from the experimental studies is whether the HIF1α/OATPs signaling axis participates in the clinical tumor imaging by NIRF dyes. To address this issue, we applied MHI-148 dye to detect clear cell RCC (CCRCC) in three complete nephrectomy specimens confirmed by imaging (CT and 2D/3D phase-contrast MRI) and histopathological (H&E stain) methods (Fig. S3 and Table S1). CCRCC, accounting for approximately 75% of all RCCs, is frequently characterized by the inactivation of the *VHL* tumor suppressor gene, which subsequently contributes to the stabilization of HIF1α and induction of hypoxia signaling [33]. In the present study, RCC patients underwent the surgical removal of the entire kidney, which was perfused immediately with MHI-148 dye in saline and subsequently subjected to *ex vivo* NIRF imaging. NIRF was detected specifically in the tumor regions referring to the diagnostic images in sharp contrast to the normal counterpart (Fig. 6A). With a further quantification analysis of small blocks of RCC versus normal tissues from three nephrectomy samples by normalizing NIRF intensity to tissue weight, we found up to 6-fold increase of MHI-148 dye uptake in tumor relative to normal tissues (Fig. 6B and 6C). To confirm the co-activation of HIF1α and OATPs in clinical RCC samples, we

conducted IHC analysis and demonstrated intense widespread nuclear HIF1α and cytoplasmic OATP1B3 expression in RCC samples but absent in adjacent normal tissues (Fig. 6D). These clinical observations reinforce the regulatory roles of HIF1α/OATPs signaling axis in mediating tumor uptake of NIRF dyes.

4. Discussion

In this study, we demonstrated the use of a specific group of NIRF heptamethine carbocyanines, identified originally to enable tumor-specific imaging and targeting, for assessing tumor hypoxia (Fig. 1). We also provided mechanistic insights into the preferential uptake of these NIRF dyes by cancer cells using genitourinary cancers as a representative model system. The mechanisms primarily involve the activation of hypoxia signaling through a key transcription factor, HIF1α, which is frequently observed in a variety of types of cancers and often associated with a poor prognosis and rapid disease progression expressing aggressive phenotypes [24]. Currently, few biomarkers to reliably detect and predict tumor hypoxia are available for clinical use, and therefore extending the application of these NIRF dyes for assessing tumor hypoxia and predicting hypoxia-regulated disease prognosis in cancer patients merits further exploration.

In a subsequent analysis of our imaging results, we compared in parallel MHI-148 with indocyanine green (ICG), the only NIRF agent approved by the Food and Drug Administration in the United States for clinical application. ICG functions *in vivo* primarily through binding to plasma proteins and enables tumor diagnosis by NIRF lymphatic imaging [34, 35], but there is little evidence showing its direct association with tumor hypoxia. Regarding the tumor-to-background ratio of NIRF signals at 24 hours for tumor detection in mice, ICG has a ratio of 1.4–1.7 [36], whereas MHI-148 shows a median of 9.1, which can be further exacerbated by 2 fold in the presence of HIF1α protein overexpression, suggesting that tumor hypoxia is an important mechanism for facilitating tumor detection by NIRF imaging. In addition, another mechanism that may contribute to the preferential accumulation of contrast agents in tumors is the disorganized tumor vasculature that can coincidentally result from tumor hypoxia [37, 38], which is able to activate the expression of VEGF to further increase vascular disorganization [24]. This scenario supports our mechanistic findings and also provides a rationale for elucidating the advantages of our dyes over other NIRF agents for cancer imaging.

We find that a group of *OATP* genes induced by hypoxia participate in mediating the uptake of NIRF dyes in cancer cells, which can be either dependent or independent from hypoxia signaling. OATPs function in the uptake of amphipathic compounds, including drugs, hormones, and other xenobiotics that cannot freely diffuse through cellular membranes, and can be either tissue-specific or expressed ubiquitously [29]. Recent studies have implicated altered *OATP* expressions and variants in many different types of cancers [30], including OATP1B3 that can serve as a testosterone transporter in PCa [39]. Our study showed the correlation of OATP1B3 expression with HIF1α expression as well as PCa progression, providing a rationale for its role in mediating the uptake of NIRF dyes by cancer cells (Fig. 4 and Fig. 5). An important finding of our study is that HIF1α directly upregulates *OATP*s, which is supported by the co-expression of these two proteins in clinical prostate and renal

cancer samples (Fig. 4 and Fig. 6). Under hypoxic conditions, active nuclear HIF1α protein interacts with a HRE in the *OATP1B3* promoter, resulting in the increased transcription of *OATP1B3* (Fig. 4). HIF1α is destabilized under normoxia due to the rapid degradation initiated by the PHD/VHL pathway [27], which is likely a mechanism responsible for the relatively low levels of OATPs in normal tissues (Supplemental Fig. 2). Hence, inactivation of HIF1α/OATPs signaling in normal cells and tissues blunts their sensitivity to recruit NIRF dyes; conversely, NIRF dyes acquire the ability to target hypoxic cancer cells. Although we used PCa as the major model system in the present study, these mechanistic findings could be extended to other types of cancers by determining the potential concerted effects exerted by HIF1α along with other OATPs on the uptake of NIRF dyes in future studies. In addition, the mechanisms by which NIRF dyes are specifically taken up by cancer cells may extend beyond the present study, and further investigation is warranted to explore other properties of NIRF dyes for targeting cancer cells, such as their long-lasting retention and preferential organelle-specific cellular localization in cancer cells.

It has been shown that NIRF heptamethine carbocyanines enter cells and form complexes with nucleic acids [40, 41] or proteins [42, 43] through non-covalent interactions, which might be potentially modulated by hypoxia either in the tumor cells or the microenvironment. Further investigation would advance our understanding of this process. To delineate the functional groups associated with dye uptake by cancer cells, the structure-activity properties of these dyes were closely examined. The bridging atoms between the two aromatic heterocycles serve as a part of rigid cyclic ring which allows conformational stability and enhanced excitations/emission properties. The nitrogen atom in heterocyclic rings is amenable for modification to a variety of functional groups including negatively-charged carboxylic acid, sulfonic acid as well as uncharged alcohol, amine and ester, which can be used for manipulating physical properties of NIRF dyes such as water solubility and conjugation with other molecular entities [44, 45]. We found that the charged dyes were well retained in cancer cells with intact imaging capability by observing fluorescence signals, while the uncharged dyes were shown to be inactive with poor retention in cells. Further chemical modifications of the functionally charged moieties via covalent conjugation with either ligands for radiolabeling or drugs showed minimal effects on their cancer-specific propensity [46, 47] and anti-cancer activity [45, 48] in tumor xenografts in mice. Moreover, structural modifications of the two heteroaromatic rings or the central meso position of the cyclohexyl ring seemed to retain the activity of NIRF dyes as well. In addition to the direct chemical modifications, the mechanistic insights provided in the present study may also shed light on the dye activity. Specifically, the potential effect of hypoxia on the net charge of dye molecules by regulating either intracellular or extracellular pH conditions may need to be taken into account for future improvements in the design of NIRF imaging dyes [49, 50]. Following these observations, we anticipate that chemical modifications of this attractive class of NIRF imaging agents will produce a wide variety of cancer imaging and targeting agents in the near future.

5. Conclusions

In this study, we elucidated the molecular mechanisms underlying the uptake of a specific class of NIRF dyes by cancer cells through hypoxia and activation of a HIF1α/OATPs

signaling axis, which provides a mechanistic rationale for targeting tumor hypoxia and cancer cells with these NIRF dyes. These findings also have great significance for the future development and application of NIRF agents in the clinic for better cancer detection, prognosis and therapy.

Supplementary Material

Refer to Web version on PubMed Central for supplementary material.

Acknowledgments

This work was supported by NIH/NCI Grant 5P01CA098912, R01CA122602, the Board of Governors Cancer Research Chair and Steven Spielberg Fund in Prostate Cancer Research (L.W-K.C.), and by the Program of International Science and Technology Cooperation of China (No. 2011DFA33110) (C.S.). We thank Dr. Lei Zhang (Fourth Military Medical University, Xi'an, Shaanxi, China) for providing clinical specimens, and Chunyan Liu for providing technical assistance. We also thank Mr. Gary Mawyer for editorial assistance.

References

1. Wu J, Pan D, Chung LW. Near-infrared fluoresence and nuclear imaging and targeting of prostate cancer. Transl Androl Urol. 2014; 2:254–264.
2. Frangioni JV. In vivo near-infrared fluorescence imaging. Curr Opin Chem Biol. 2003; 7:626–634. [PubMed: 14580568]
3. Rao J, Dragulescu-Andrasi A, Yao H. Fluorescence imaging in vivo: recent advances. Curr Opin Biotechnol. 2007; 18:17–25. [PubMed: 17234399]
4. Hawrysz DJ, Sevick-Muraca EM. Developments toward diagnostic breast cancer imaging using near-infrared optical measurements and fluorescent contrast agents. Neoplasia. 2000; 2:388–417. [PubMed: 11191107]
5. Hintersteiner M, Enz A, Frey P, Jaton AL, Kinzy W, Kneuer R, et al. In vivo detection of amyloid-beta deposits by near-infrared imaging using an oxazine-derivative probe. Nat Biotechnol. 2005; 23:577–583. [PubMed: 15834405]
6. Wu X, Liu H, Liu J, Haley KN, Treadway JA, Larson JP, et al. Immunofluorescent labeling of cancer marker Her2 and other cellular targets with semiconductor quantum dots. Nat Biotechnol. 2003; 21:41–46. [PubMed: 12459735]
7. Humblet V, Lapidus R, Williams LR, Tsukamoto T, Rojas C, Majer P, et al. High-affinity near-infrared fluorescent small-molecule contrast agents for in vivo imaging of prostate-specific membrane antigen. Mol Imaging. 2005; 4:448–462. [PubMed: 16285907]
8. Frangioni JV. New technologies for human cancer imaging. J Clin Oncol. 2008; 26:4012–4021. [PubMed: 18711192]
9. Pierce MC, Javier DJ, Richards-Kortum R. Optical contrast agents and imaging systems for detection and diagnosis of cancer. Int J Cancer. 2008; 123:1979–1990. [PubMed: 18712733]
10. Edwards PA. Heterogeneous expression of cell-surface antigens in normal epithelia and their tumours, revealed by monoclonal antibodies. Br J Cancer. 1985; 51:149–160. [PubMed: 2578284]
11. Yang X, Shi C, Tong R, Qian W, Zhau HE, Wang R, et al. Near IR heptamethine cyanine dye-mediated cancer imaging. Clin Cancer Res. 2010; 16:2833–2844. [PubMed: 20410058]
12. Yang X, Shao C, Wang R, Chu CY, Hu P, Master V, et al. Optical imaging of kidney cancer with novel near infrared heptamethine carbocyanine fluorescent dyes. J Urol. 2013; 189:702–710. [PubMed: 23000848]
13. Zhau HY, Chang SM, Chen BQ, Wang Y, Zhang H, Kao C, et al. Androgen-repressed phenotype in human prostate cancer. Proc Natl Acad Sci U S A. 1996; 93:15152–15157. [PubMed: 8986779]
14. Zhau HE, Odero-Marah V, Lue HW, Nomura T, Wang R, Chu G, et al. Epithelial to mesenchymal transition (EMT) in human prostate cancer: lessons learned from ARCaP model. Clin Exp Metastasis. 2008; 25:601–610. [PubMed: 18535913]

15. Wu HC, Hsieh JT, Gleave ME, Brown NM, Pathak S, Chung LW. Derivation of androgen-independent human LNCaP prostatic cancer cell sublines: role of bone stromal cells. Int J Cancer. 1994; 57:406–412. [PubMed: 8169003]
16. Qi J, Tripathi M, Mishra R, Sahgal N, Fazli L, Ettinger S, et al. The E3 ubiquitin ligase Siah2 contributes to castration-resistant prostate cancer by regulation of androgen receptor transcriptional activity. Cancer Cell. 2013; 23:332–346. [PubMed: 23518348]
17. Wu JB, Chen K, Li Y, Lau YF, Shih JC. Regulation of monoamine oxidase A by the SRY gene on the Y chromosome. Faseb J. 2009; 23:4029–4038. [PubMed: 19661285]
18. Sahu D, Zhao Z, Tsen F, Cheng CF, Park R, Situ AJ, et al. A potentially common peptide target in secreted heat shock protein-90alpha for hypoxia-inducible factor-1alpha-positive tumors. Mol Biol Cell. 2012; 23:602–613. [PubMed: 22190738]
19. Hu P, Chu GC, Zhu G, Yang H, Luthringer D, Prins G, et al. Multiplexed quantum dot labeling of activated c-Met signaling in castration-resistant human prostate cancer. PLoS One. 2011; 6:e28670. [PubMed: 22205960]
20. Chen K, Ou XM, Wu JB, Shih JC. Transcription factor E2F–associated phosphoprotein (EAPP), RAM2/CDCA7L/JPO2 (R1), and simian virus 40 promoter factor 1 (Sp1) cooperatively regulate glucocorticoid activation of monoamine oxidase B. Molecular pharmacology. 2011; 79:308–317. [PubMed: 20980443]
21. Livak KJ, Schmittgen TD. Analysis of relative gene expression data using real-time quantitative PCR and the 2(-Delta Delta C(T)) Method. Methods. 2001; 25:402–408. [PubMed: 11846609]
22. Wu JB, Chen K, Ou XM, Shih JC. Retinoic acid activates monoamine oxidase B promoter in human neuronal cells. J Biol Chem. 2009; 284:16723–16735. [PubMed: 19401466]
23. Wu JB, Shih JC. Valproic acid induces monoamine oxidase A via Akt/forkhead box O1 activation. Mol Pharmacol. 2011; 80:714–723. [PubMed: 21775495]
24. Lu X, Kang Y. Hypoxia and hypoxia-inducible factors: master regulators of metastasis. Clin Cancer Res. 2010; 16:5928–5935. [PubMed: 20962028]
25. Ameri K, Luong R, Zhang H, Powell AA, Montgomery KD, Espinosa I, et al. Circulating tumour cells demonstrate an altered response to hypoxia and an aggressive phenotype. Br J Cancer. 2010; 102:561–569. [PubMed: 20051957]
26. Harada H, Kizaka-Kondoh S, Itasaka S, Shibuya K, Morinibu A, Shinomiya K, et al. The combination of hypoxia-response enhancers and an oxygen-dependent proteolytic motif enables real-time imaging of absolute HIF-1 activity in tumor xenografts. Biochem Biophys Res Commun. 2007; 360:791–796. [PubMed: 17624305]
27. Kaelin WG Jr, Ratcliffe PJ. Oxygen sensing by metazoans: the central role of the HIF hydroxylase pathway. Mol Cell. 2008; 30:393–402. [PubMed: 18498744]
28. Li J, Shi M, Cao Y, Yuan W, Pang T, Li B, et al. Knockdown of hypoxia-inducible factor-1alpha in breast carcinoma MCF-7 cells results in reduced tumor growth and increased sensitivity to methotrexate. Biochem Biophys Res Commun. 2006; 342:1341–1351. [PubMed: 16516853]
29. Obaidat A, Roth M, Hagenbuch B. The expression and function of organic anion transporting polypeptides in normal tissues and in cancer. Annu Rev Pharmacol Toxicol. 2012; 52:135–151. [PubMed: 21854228]
30. Pressler H, Sissung TM, Venzon D, Price DK, Figg WD. Expression of OATP family members in hormone-related cancers: potential markers of progression. PLoS One. 2011; 6:e20372. [PubMed: 21625523]
31. Yang M, Xie W, Mostaghel E, Nakabayashi M, Werner L, Sun T, et al. SLCO2B1 and SLCO1B3 may determine time to progression for patients receiving androgen deprivation therapy for prostate cancer. J Clin Oncol. 2011; 29:2565–2573. [PubMed: 21606417]
32. Semenza GL, Agani F, Booth G, Forsythe J, Iyer N, Jiang BH, et al. Structural and functional analysis of hypoxia-inducible factor 1. Kidney Int. 1997; 51:553–555. [PubMed: 9027737]
33. Zbar B, Klausner R, Linehan WM. Studying cancer families to identify kidney cancer genes. Annu Rev Med. 2003; 54:217–233. [PubMed: 12525673]
34. Hirche C, Murawa D, Mohr Z, Kneif S, Hunerbein M. ICG fluorescence-guided sentinel node biopsy for axillary nodal staging in breast cancer. Breast Cancer Res Treat. 2010; 121:373–378. [PubMed: 20140704]

35. Cherrick GR, Stein SW, Leevy CM, Davidson CS. Indocyanine green: observations on its physical properties, plasma decay, and hepatic extraction. J Clin Invest. 1960; 39:592–600. [PubMed: 13809697]
36. Kosaka N, Mitsunaga M, Longmire MR, Choyke PL, Kobayashi H. Near infrared fluorescence-guided real-time endoscopic detection of peritoneal ovarian cancer nodules using intravenously injected indocyanine green. Int J Cancer. 2011; 129:1671–1677. [PubMed: 21469142]
37. Less JR, Skalak TC, Sevick EM, Jain RK. Microvascular architecture in a mammary carcinoma: branching patterns and vessel dimensions. Cancer Res. 1991; 51:265–273. [PubMed: 1988088]
38. Jin H, Kang KA. Fluorescence-mediated detection of a heterogeneity in a highly scattering media. Adv Exp Med Biol. 2005; 566:167–172. [PubMed: 16594149]
39. Hamada A, Sissung T, Price DK, Danesi R, Chau CH, Sharifi N, et al. Effect of SLCO1B3 haplotype on testosterone transport and clinical outcome in caucasian patients with androgen-independent prostatic cancer. Clin Cancer Res. 2008; 14:3312–3318. [PubMed: 18519758]
40. Ihmels H, Thomas L. Light up G-quadruplex DNA with a [2.2.2]heptamethinecyanine dye. Organic & biomolecular chemistry. 2013; 11:480–487. [PubMed: 23203349]
41. Karlsson HJ, Eriksson M, Perzon E, Akerman B, Lincoln P, Westman G. Groove-binding unsymmetrical cyanine dyes for staining of DNA: syntheses and characterization of the DNA-binding. Nucleic acids research. 2003; 31:6227–6234. [PubMed: 14576310]
42. Volkova KD, Kovalska VB, Balanda AO, Vermeij RJ, Subramaniam V, Slominskii YL, et al. Cyanine dye-protein interactions: looking for fluorescent probes for amyloid structures. Journal of biochemical and biophysical methods. 2007; 70:727–733. [PubMed: 17467807]
43. Patonay G, Kim JS, Kodagahally R, Strekowski L. Spectroscopic study of a novel bis(heptamethine cyanine) dye and its interaction with human serum albumin. Applied spectroscopy. 2005; 59:682–690. [PubMed: 15969815]
44. Yeh CS, Su CH, Ho WY, Huang CC, Chang JC, Chien YH, et al. Tumor targeting and MR imaging with lipophilic cyanine-mediated near-infrared responsive porous Gd silicate nanoparticles. Biomaterials. 2013; 34:5677–5688. [PubMed: 23639532]
45. Henary M, Pannu V, Owens EA, Aneja R. Near infrared active heptacyanine dyes with unique cancer-imaging and cytotoxic properties. Bioorganic & medicinal chemistry letters. 2012; 22:1242–1246. [PubMed: 22177785]
46. Zhang Y, Xiao L, Popovic K, Xie X, Chordia MD, Chung LW, et al. Novel cancer-targeting SPECT/NIRF dual-modality imaging probe (99m)Tc-PC-1007: synthesis and biological evaluation. Bioorganic & medicinal chemistry letters. 2013; 23:6350–6354. [PubMed: 24125889]
47. Xiao L, Zhang Y, Yue W, Xie X, Wang JP, Chordia MD, et al. Heptamethine cyanine based (64)Cu-PET probe PC-1001 for cancer imaging: synthesis and in vivo evaluation. Nuclear medicine and biology. 2013; 40:351–360. [PubMed: 23375364]
48. Tan X, Luo S, Wang D, Su Y, Cheng T, Shi C. A NIR heptamethine dye with intrinsic cancer targeting, imaging and photosensitizing properties. Biomaterials. 2012; 33:2230–2239. [PubMed: 22182749]
49. Hulikova A, Harris AL, Vaughan-Jones RD, Swietach P. Regulation of intracellular pH in cancer cell lines under normoxia and hypoxia. Journal of cellular physiology. 2013; 228:743–752. [PubMed: 22949268]
50. Brahimi-Horn MC, Pouyssegur J. Hypoxia in cancer cell metabolism and pH regulation. Essays in biochemistry. 2007; 43:165–178. [PubMed: 17705800]

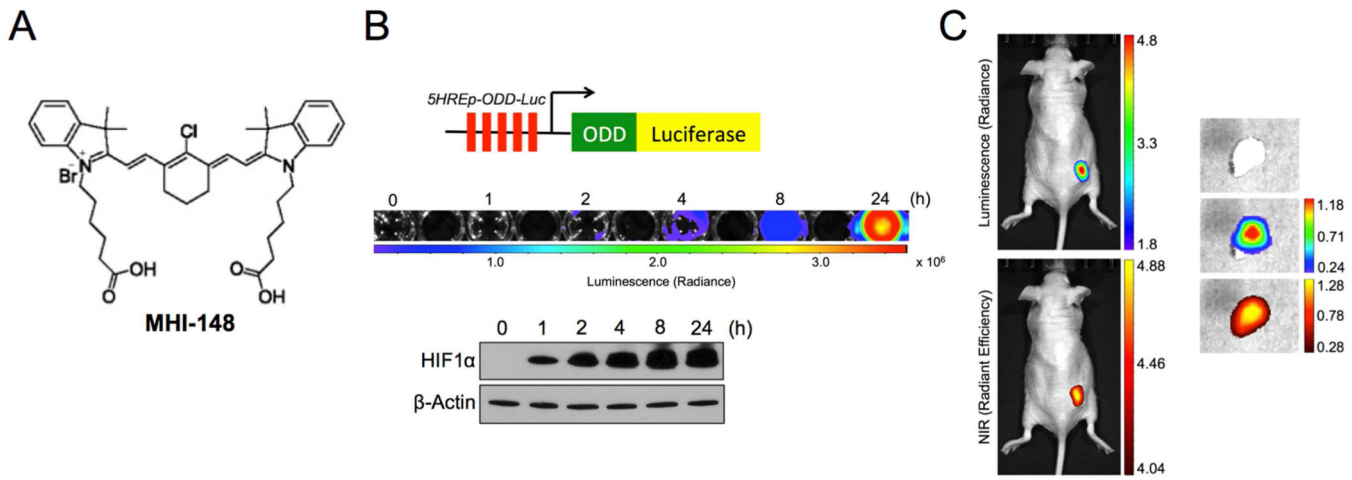

Fig. 1.

MHI-148, a NIRF dye, assessed tumor hypoxia. (A) Chemical structure of NIR heptamethine carbocyanine MHI-148 dye. (B) Generation and validation of human PCa PC-3 cells that stably expressed the *5HRE-pODD-Luc* construct (top). Stable cells were treated with hypoxia (1% O_2) for different times as indicated and then subjected to either luminescence imaging (middle) or immunoblotting of HIF1α protein expression (bottom). (C) *In vivo* and ex *vivo* images of PC-3 tumor xenografts that expressed *5HRE-pODD-Luc* construct by both bioluminescence (top) and NIRF (bottom) imaging, which showed superimposed signal distribution. Scale bars represent $x10^5$ and $x10^9$ for *in vivo* bioluminescence and NIRF, respectively; $x10^4$ and $x10^9$ for *ex vivo* bioluminescence and NIRF, respectively, in the unit of radiant efficiency.

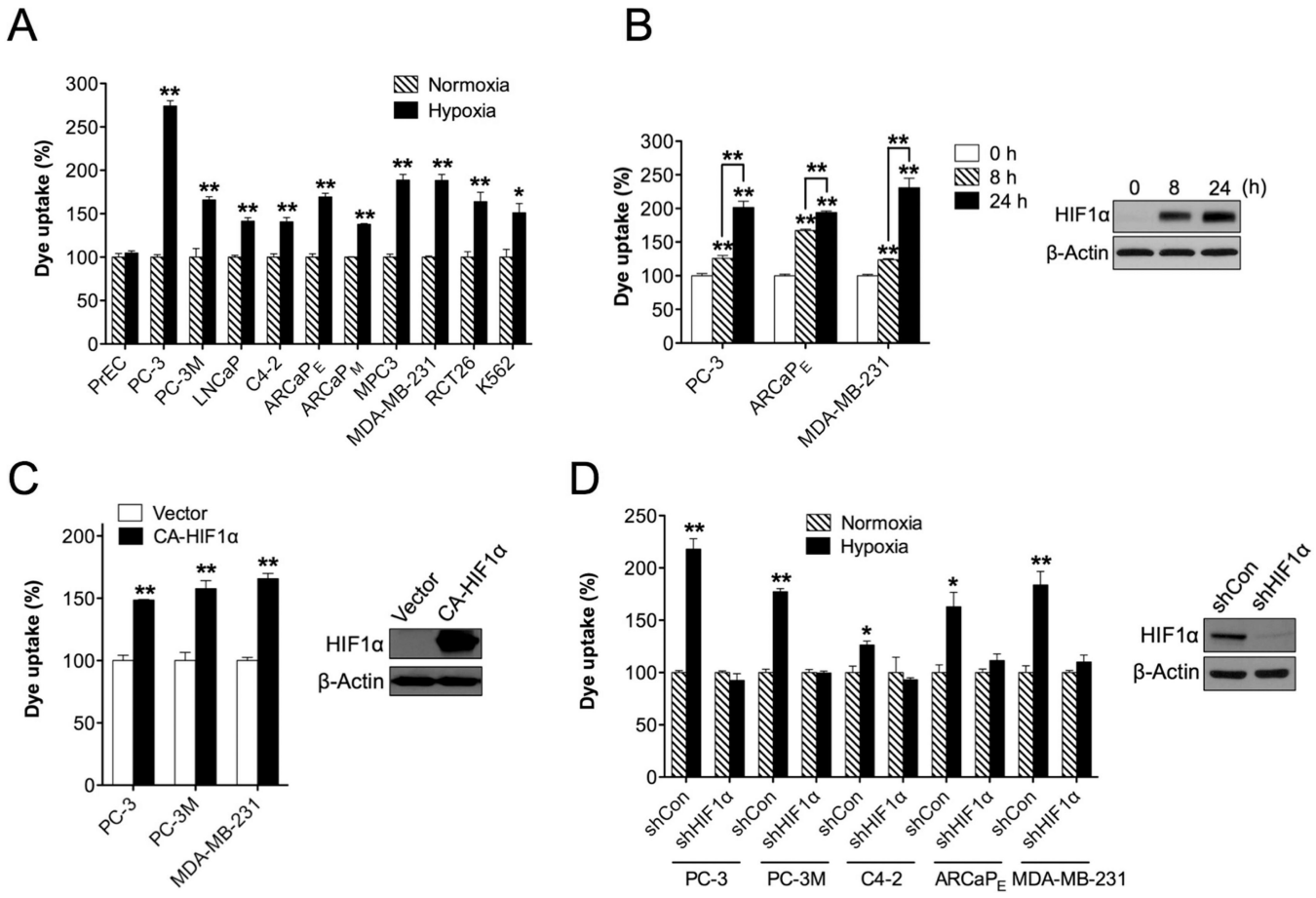

Fig. 2.

Hypoxia and HIF1α mediated the uptake of MHI-148 dye by cancer cells. (A) Determination of MHI-148 dye uptake in multiple cancer cell lines under either normoxic or hypoxic (1% O_2, 4 hr) conditions (N=3, mean ± SEM). Normal human prostatic epithelial PrEC cells were used as a negative control. Dye uptake by cells under normoxia was set as 100%. (B) Determination of MHI-148 dye uptake in select cancer cell lines under $CoCI_2$ (200 μM) treatment for different time periods as indicated (N=3, mean ± SEM). The $CoCI_2$ effect in PC-3 cells as a representative was examined by immunoblotting HIF1α protein expression. (C, D) Determination of MHI-148 dye uptake in cancer cells either overexpressing constitutively active HIF1α (C) or with stable knockdown of HIF1α (D) (N=3, mean ± SEM). The efficacy of overexpression or knockdown of HIF1α in PC-3 cells as a representative was examined by immunoblotting HIF1α protein expression. *p<0.05, **p<0.01.

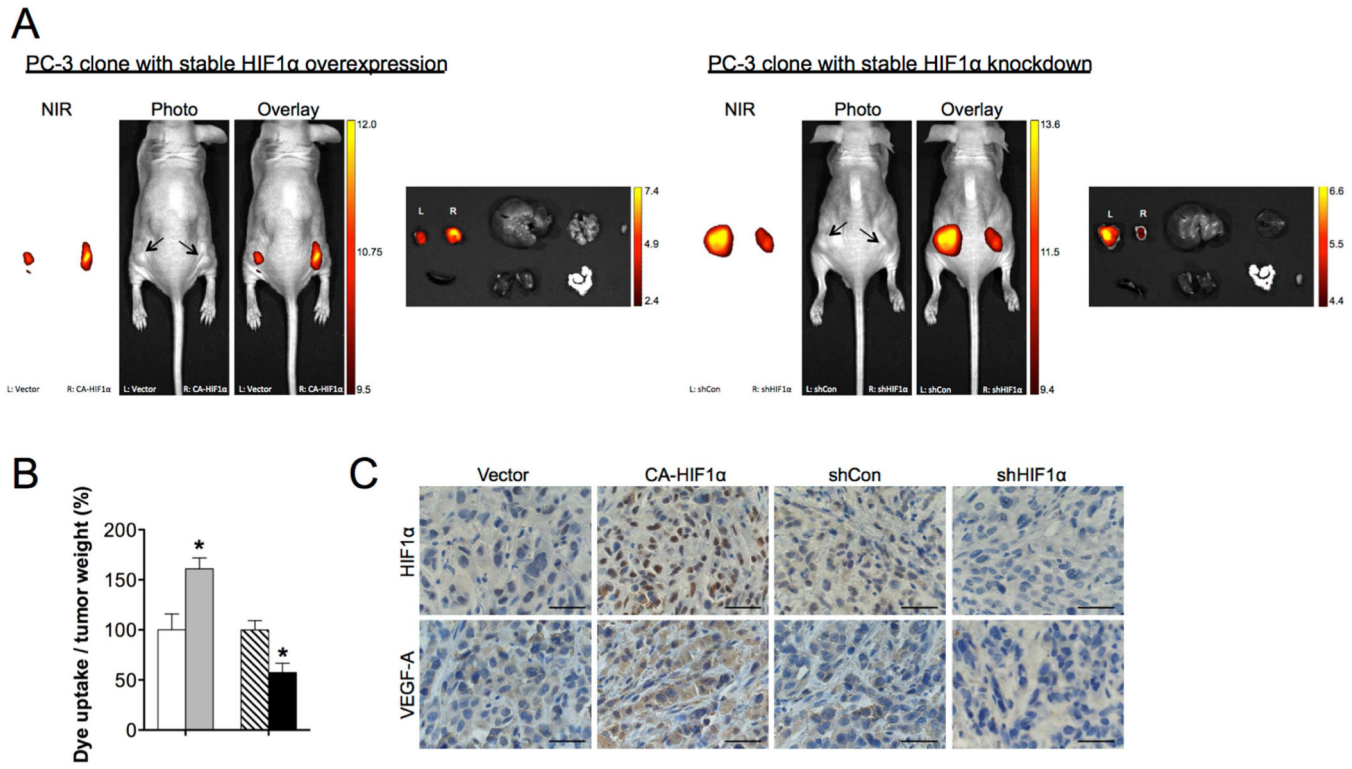

Fig. 3.

Hypoxia and HIF1α mediated the uptake of MHI-148 dye by tumor xenografts. (A) Representative *in vivo* and ex *vivo* NIRF images of control (left flank) vs. HIF1α-overexpressing (right flank) (left panel) and control (left flank) vs. HIFIα-knockdown (right flank) (right panel) PC-3 tumor xenografts. Scale bars represent $x10^8$ for both *in vivo* and ex *vivo* NIRF in the unit of radiant efficiency. (B) Quantitation of tumor uptake of MHI-148 dye (N=5, mean ± SEM) presented as the ratio of dye intensity to tumor weight. *p<0.05, **p<0.01. (C) IHC analysis of HIF1α and VEGF-A expression in PC-3 tumor xenografts with different manipulation of HIF1α levels as indicated. Representative images are shown. Original magnification, x400; scale bars represent 20 μm.

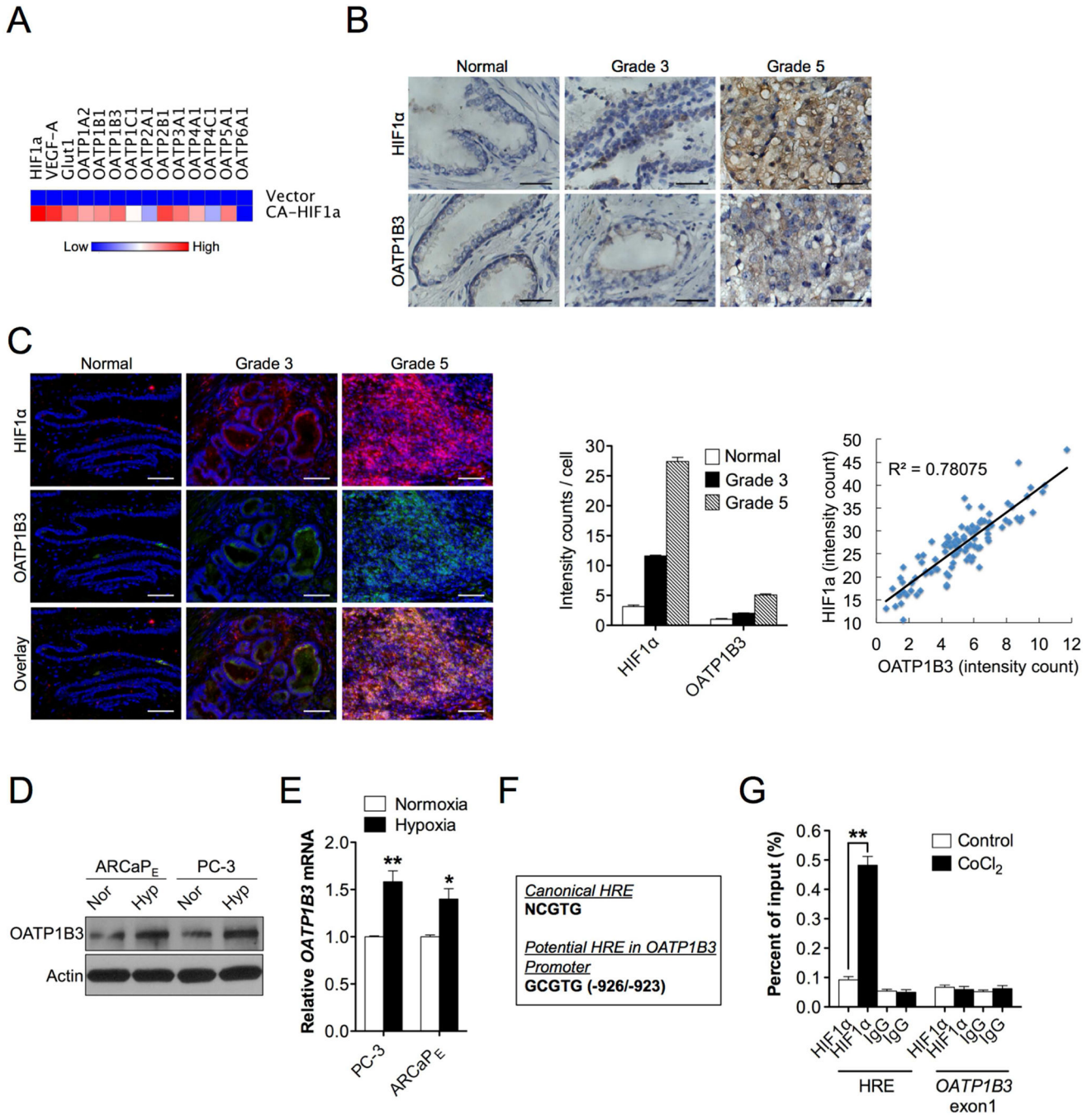

Fig. 4.

Co-expression and regulation of HIF1α and OATPs in human PCa. (A) Heat map depicting OATPs mRNA expression profiling in constitutively active HIF1α-overexpressing PC-3 cells by qPCR. (B, C) IHC (B) and double QDL (C, left panel) staining of HIF1α and OATP1B3 expression in clinical specimens of normal prostatic epithelium, Gleason grade 3 and 5 PCa (N=15 for each). Representative images are shown. Original magnification, x400; scale bars represent 20 μm. Cell-based average intensity counts of HIF1α and OATP1B3 stain from 1,000 each of normal, grade 3 and 5 samples were quantified using in Form

software (C, middle panel). Intensity of HIF1α and OATP1B3 co-expression in 100 single cells from a representative high-grade individual patient was analyzed for gene expression correlation (C, right panel). (D, E) Determination of OATP1B3 protein (D) and mRNA (E) expression in PC-3 and $ARCaP_E$ cells in response to hypoxia (1% O_2) for 24 hrs and 4 hrs, respectively. (F) Sequences of the canonical HRE (top sequence) and a potential HRE in *OATP1B3* promoter (bottom sequence). (G) Chromatin from either vehicle- or $CoCI_2$-treated (200 μM, 16 hr) PC-3 cells was immunoprecipitated using anti-HIF1α or IgG antibodies followed by qPCR using 1 primer set for the HRE in *OATP1B3* promoter and 1 control primer set for *0ATP1B3* exonl. Data represent the mean ± SEM of three separate experiments. *p<0.05, **p<0.01.

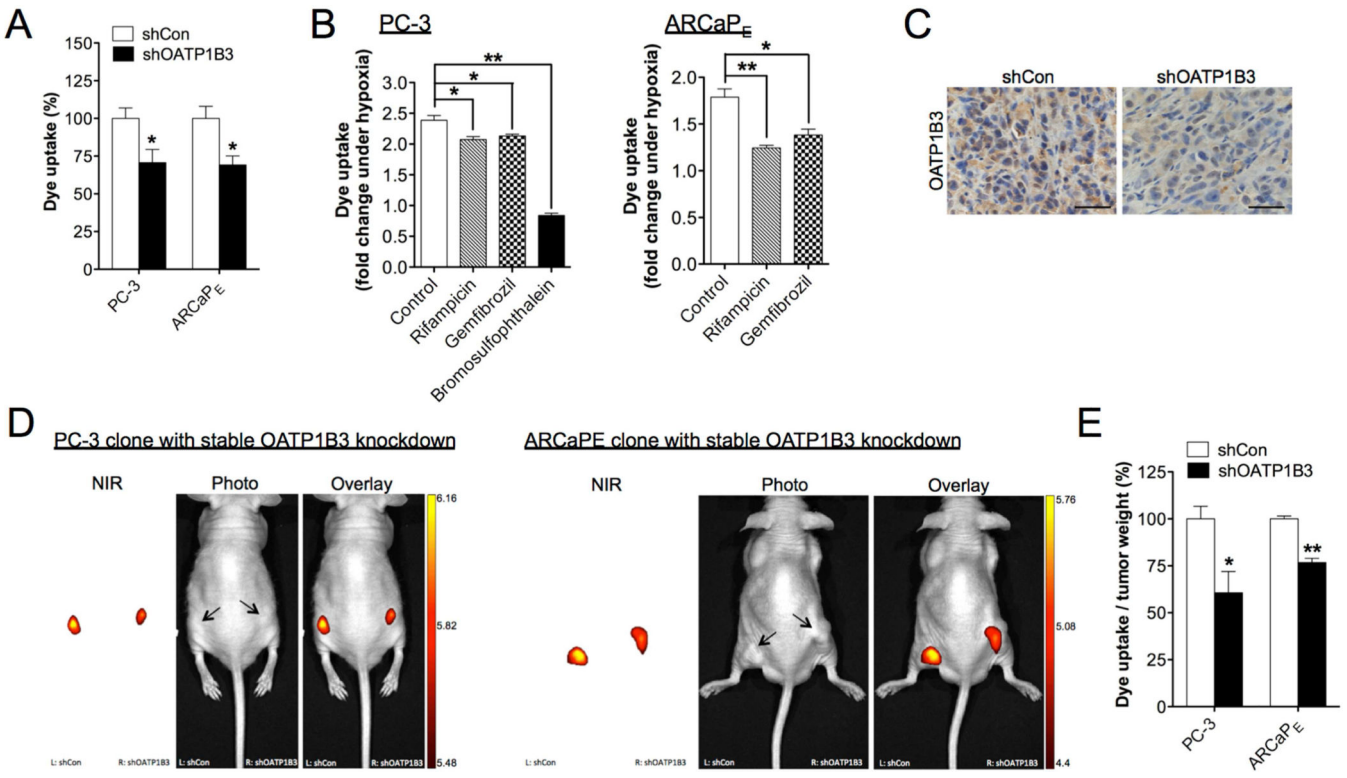

Fig. 5.

OATP1B3 mediated the uptake of MHI-148 dye by cancer cells and tumor xenografts. (A) Determination of MHI-148 dye uptake in PC-3 and $ARCaP_E$ cells with stable knockdown of OATP1B3 (N=3, mean ± SEM). (B) Determination of MHI-148 dye uptake in PC-3 (left panel) and $ARCaP_E$ (right panel) cells pre-treated with different OATP1B3 selective inhibitors as indicated for 1 hr followed by hypoxia treatment (1% O_2, 4 hr). Data was presented as fold change of MHI-148 dye uptake with hypoxia (N=3, mean ± SEM). (C) IHC analysis of OATP1B3 expression in control and OATP1B3-knockdown PC-3 tumor xenograft. Original magnification, x400; scale bars represent 20 μm. (D) Representative *in vivo* NIRF images of control (left flank)/OATP1B3-knockdown (right flank) PC-3 (left panel) and $ARCaP_E$ (right panel) tumor xenografts. Scale bars represent $x10^9$ for *in vivo* NIRF imaging of both PC-3 and $ARCaP_E$ tumor xenografts in the unit of radiant efficiency. (E) Quantitation of MHI-148 dye uptake in tumor xenografts (N=5, mean ± SEM), presented as the ratio of dye intensity to tumor weight. *p<0.05, **p<0.01.

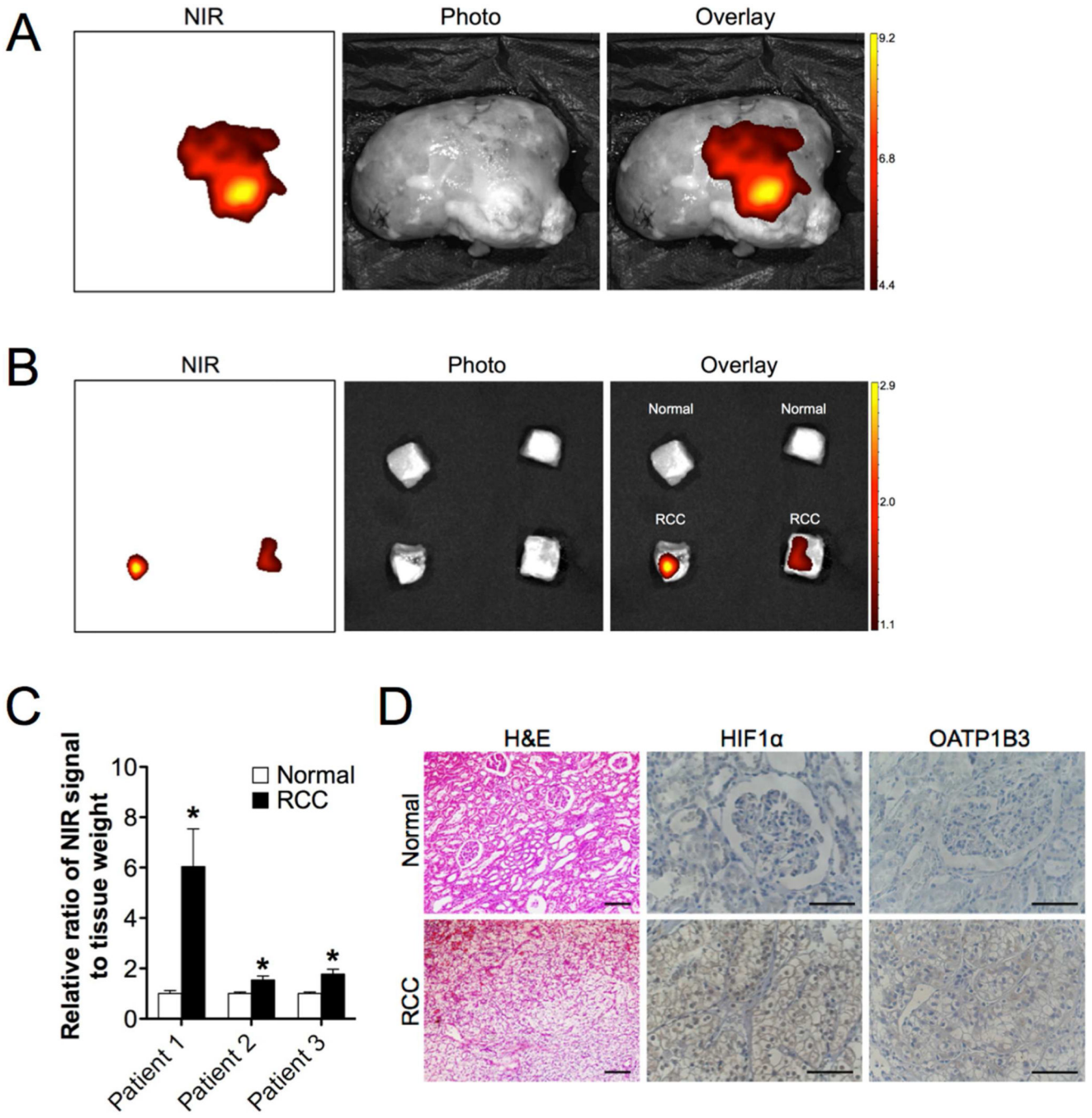

Fig. 6.

NIRF imaging of clinical RCC samples. (A, B) Representative NIRF images of excised kidney by complete nephrectomy (A) as well as small cuts of normal (B, top) and RCC tissues (B, bottom) from an individual patient. Scale bars represent $x10^9$ and $x10^8$ for (A) and (B), respectively, in the unit of radiant efficiency. (C) Quantitation of MHI-148 dye uptake in normal and tumor tissues from three RCC patients, presented as the ratio of dye intensity to tissue weight from five cuts of tissues of each patient (mean ± SEM). (D) H&E stain and IHC analysis of HIF1α and OATP1B3 expression in normal and RCC samples.

Representative images are shown. Original magnification, x200 (H&E) and x400 (IHC); scale bars represent 20 μm. *p<0.05.